Surface-plasmon dispersion relations in chains of metallic nanoparticles: An exact quasistatic calculation

Sung Yong Park and David Stroud
Department of Physics, The Ohio State University, Columbus, Ohio 43210, USA
(Received 14 November 2003; published 29 March 2004)

We calculate the surface-plasmon dispersion relations for a periodic chain of spherical metallic nanoparticles in an isotropic host, including all multipole modes, in a generalized tight-binding approach. For sufficiently small particles ($kd \ll 1$, where k is the wave vector and d is the interparticle separation), the calculation is exact. The lowest bands differ only slightly from previous point-dipole calculations provided the particle radius $a \lesssim d/3$, but differ substantially at smaller separation. We also calculate the dispersion relations for many higher bands, and estimate the group velocity v_g and the exponential decay length ξ_D for energy propagation for the lowest two bands due to single-grain damping. For $a/d = 0.33$, the result for ξ_D is in qualitative agreement with experiments on gold nanoparticle chains, while for smaller separation, such as $a/d = 0.45$, v_g and ξ_D are expected to be strongly k dependent because of the multipole corrections. When the particles touch, we predict percolation effects in the spectrum, and find surprising symmetry in the plasmon band structure. Finally, we reformulate the band-structure equations for a Drude metal in the time domain, and suggest how to include localized driving electric fields in the equations of motion.

DOI: 10.1103/PhysRevB.69.125418 PACS number(s): 78.67.Bf, 42.79.Gn, 71.45.Gm, 73.20.Mf

I. INTRODUCTION

Recently, it has been shown that energy can be transmitted along a one-dimensional (1D) chain of equally spaced metallic nanoparticles, via propagating surface-plasmon (SP) modes.[1–8] These modes are basically linear combinations of single-grain SP modes, i.e., oscillations of electronic charge within a single grain.[9] The single-grain modes are accompanied by an oscillating electric moment (dipole and higher) on the grain. The electric field of this moment in turn generates oscillating moments on neighboring spheres.

The propagating SP modes are simply traveling waves of these oscillating moments. They are characterized by well defined dispersion relations $\omega(k)$ which relate their frequencies ω and wave vectors k.[2,3] If the damping is sufficiently small, the energy transmitted by these ways may travel at speeds up to $0.1c$. Thus, one can imagine a variety of possible uses for these waves.

The calculation of $\omega(k)$ typically involves several approximations. The first of these is the *near field* approximation—that is, one assumes that $kd \ll 1$, where k is the wave number and d the interparticle separation. This assumption permits the electric field **E** to be calculated in the quasistatic limit, in which **E** is expressed as the gradient of a scalar potential.

A second common approximation is that the field produced by a given particle at its neighbors is that of a *point dipole*. However, this second assumption is stronger than the quasistatic approximation, and becomes inaccurate when the particles are closely spaced. Under these conditions, the quasistatic fields may be modified significantly by multipolar interactions. Typically, these multipolar fields have been included by numerical techniques such as finite-difference time-domain calculations. However, it may be difficult to obtain accurate results by these numerical techniques, because the higher multipole excitations may produce fields which vary rapidly in space, whereas numerical studies with insufficient discretization may not achieve adequate resolution. Thus, an exact calculation in a simple geometry may not only provide physical insights into this system, but also gives useful guidelines for the validity of numerical calculations in more complex geometries.

In the present work, we will show how these multipolar corrections can be calculated *exactly*, using a straightforward analytical approach. The formalism is analogous to the generalized tight-binding method in conventional band theory. In this approach, one constructs Bloch states from individual atomic orbitals, and then diagonalizes the Hamiltonian matrix in the basis of these atomic orbitals. In the surface-plasmon analog, the individual atomic orbitals are multipolar SP oscillations for each sphere. The matrix elements needed to calculate the Hamiltonian matrix are easily constructed, especially for a periodic 1D chain of spheres. The diagonalization needed to calculate the bands is readily carried out. The entire calculation is made simpler in 1D systems, because the Hamiltonian matrix decomposes into separate blocks, one for each azimuthal quantum number m.

The basic formalism necessary to carry out this calculation[10] has thus far been applied only rather sparingly, because there have been few experimentally available realizations of the ordered geometry required for this approach. It has been applied mainly to calculating the effective complex dielectric function $\epsilon_e(\omega)$ of a periodic composite medium, which requires the SP band structure only at Bloch vector $\mathbf{k} = 0$. Only recently has it become possible to produce well-controlled ordered metallic structures at the nanoscale, and hence to generate and detect these SP waves at general wave vectors. In this paper, we describe and numerically solve the equation necessary to calculate this band structure in the general case of $\mathbf{k} \neq 0$ in 1D systems.

Besides giving the solutions in the full multipolar case,

we also include damping of the SP modes due to losses within the individual metallic particles. For a Drude metal, these losses can be treated by including a finite relaxation time τ in the Drude dielectric function. This damping can be included approximately by adding an imaginary part to the SP frequencies. We also briefly discuss why the damping due to radiative energy losses is expected to be small. These losses arise from the breakdown of the quasistatic approximation, and can, in principle, also be approximately included by adding an imaginary part to the surface-plasmon frequency.

We will also present the multipolar SP equations in the *time* domain for a Drude metal, where they take the form of a set of coupled second-order ordinary differential equations. In this form, it is straightforward to include single-particle damping (and also, in principle, radiative damping). Moreover, one can also incorporate driving terms, arising, e.g., from external electric fields. These equations may thus be useful in modeling specific types of experimental probes which produce localized time-dependent electric fields.

The remainder of this paper is organized as follows. In Sec. II, we describe the formalism needed to calculate the SP band structure, and specialize to the calculation for a 1D chain. Section III presents numerical results in this 1D chain system. In Sec. IV, we discuss our results, and suggest some possible extensions to other geometries. Finally, the Appendix presents an alternative formulation of the equations of motion in the time domain, and describes how localized time-dependent driving electric fields can be included in these equations.

II. FORMALISM

We consider a 1D chain of spherical particles of radius a, separated by a distance d ($d \geqslant 2a$). The particles are assumed to be arranged along the z axis with centers at $z = 0, \pm d, \pm 2d, \ldots$. We assume that the particles and host have dielectric functions $\epsilon_m(\omega)$ and $\epsilon_h(\omega)$. To be definite, we may consider the particles as metallic and the host as insulating, but the discussion below applies to any choice of ϵ_m and ϵ_h. All the formalism is given in terms of a frequency variable s defined by

$$s = \frac{1}{1-\epsilon_m/\epsilon_h}. \tag{1}$$

As will be seen below, and as is discussed indirectly in Ref. 10, all the allowed propagating SP frequencies correspond to s in the range $0 \leqslant s \leqslant 1$, or equivalently, to $-\infty \leqslant \epsilon_m/\epsilon_h \leqslant 0$, assuming that ϵ_m and ϵ_h are both real.

We will calculate the SP band structure in an "atomic" basis n,ℓ,m. Here, ℓ and m label the "angular momentum" of the eigenfunction, and n labels the grain. Thus, the allowed values of these indices are $n = 0, \pm 1, \pm 2, \ldots, \ell = 1,2,3, \ldots$, and $m = -\ell, -\ell+1, \ldots, \ell$. In order to calculate the SP band structure in this basis, we first need the matrix element $Q_{n\ell m;n'\ell'm'}$, where $n \neq n'$. This matrix element is given by (see, e.g., Ref. 10)

$$\begin{aligned} Q_{n\ell m;n'\ell'm'} = (-1)^{\ell'+m'} &\left(\frac{a}{|n-n'|d}\right)^{\ell+\ell'+1} \\ &\times \left(\frac{\ell\ell'}{(2\ell+1)(2\ell'+1)}\right)^{1/2} \\ &\times \frac{(\ell+\ell'+m-m')!}{[(\ell+m)!(\ell'+m')!(\ell-m)!(\ell'-m')!]^{1/2}} \\ &\times \exp[i\phi_b(m'-m)] P_{\ell'+\ell}^{m'-m}(\cos\theta_b). \end{aligned} \tag{2}$$

Here we have introduced $\mathbf{b} = (n'-n)d\hat{z}$, which is the vector separation between the grains centered at $n'\hat{z}$ and $n\hat{z}$, and the polar and azimuthal angles θ_b and ϕ_b for this displacement vector. Since $\mathbf{b} = b\hat{z}$, θ_b is either 0 or π, depending on whether b is positive or negative. If $b > 0$, $P_{\ell'+\ell}^{m'-m} = \delta_{m',m}$, whereas if $b < 0$, $P_{\ell'+\ell}^{m'-m} = (-1)^{\ell'+\ell}\delta_{m',m}$. Incorporating these simplifications, we find that with

$$\begin{aligned} Q_{n\ell m;n'\ell'm'} = (-1)^{\ell'+m} &\left(\frac{a}{|n'-n|d}\right)^{\ell+\ell'+1} \\ &\times \left(\frac{\ell\ell'}{(2\ell+1)(2\ell'+1)}\right)^{1/2} \\ &\times \frac{(\ell+\ell')!}{[(\ell+m)!(\ell'+m)!(\ell-m)!(\ell'-m)!]^{1/2}} \\ &\times \left(\frac{n'-n}{|n'-n|}\right)^{\ell+\ell'} \delta_{m,m'}. \end{aligned} \tag{3}$$

The matrix elements are diagonal in m because the one-dimensional chain is unchanged on rotation by any angle about the z axis.

Next, we define the matrix element

$$Q_{\ell m;\ell'm'}(k) = \sum_{n\neq 0} Q_{0,\ell m;n\ell'm} \exp(inkd)\,\delta_{m,m'}, \tag{4}$$

where the sum runs over all positive and negative integers except $n = 0$. We have used the fact that, for this periodic 1D system, $Q_{n\ell m;n'\ell'm'}$ is a function only of $n-n'$ and vanishes for $m \neq m'$. After a little algebra, using Eqs. (3) and (4), we obtain

$$Q_{\ell m;\ell'm'}(k) = \left(\frac{a}{d}\right)^{\ell+\ell'+1} \sum_{n=1}^{\infty} \frac{\cos(nkd)}{n^{\ell+\ell'+1}} K_{\ell,\ell',m}\delta_{m,m'} \tag{5}$$

for $\ell+\ell'$ even, and

$$Q_{\ell m;\ell'm}(k) = \left(\frac{a}{d}\right)^{\ell+\ell'+1} \sum_{n=1}^{\infty} \frac{\sin(nkd)}{n^{\ell+\ell'+1}} K_{\ell,\ell',m}\delta_{m,m'} \tag{6}$$

for $\ell+\ell'$ odd, where

$$K_{\ell,\ell',m}=2(-1)^{\ell'+m}\left(\frac{\ell\ell'}{(2\ell+1)(2\ell'+1)}\right)^{1/2} \times\frac{(\ell+\ell')!}{[(\ell+m)!(\ell'+m)!(\ell-m)!(\ell'-m)!]^{1/2}}. \tag{7}$$

Finally, in terms of the matrix elements $Q_{\ell m\ell' m}$; the SP structure is given by

$$\det|s-H|=0, \tag{8}$$

where the ''Hamiltonian'' H has matrix elements

$$H_{\ell m;\ell' m}(k)=s_\ell\delta_{\ell,\ell'}+Q_{\ell m;\ell' m}(k), \tag{9}$$

and the ''atomic'' eigenvalues s_ℓ are given by

$$s_\ell=\frac{\ell}{2\ell+1}. \tag{10}$$

Note that $s_1=1/3$, while $s_\ell\to 1/2$ as $\ell\to\infty$.

The full SP band structure at wave vector k is obtained by diagonalizing the matrix (9). As in conventional band theory, there are many band energies for a given k, and one need consider only the bands in the first Brillouin zone, i.e., in this case, for $-\pi/d<k\leqslant\pi/d$, since the states at other values of k are equivalent to those in the first zone. For this one-dimensional system, the Hamiltonian breaks into separate blocks, one for each value of m; this conveniently reduces the size of the matrix which needs to be diagonalized. Finally, as in the linear combination of atomic orbital (LCAO) method of conventional band theory, the band structure that results from this analysis is composed of bands which originate from various atomic orbitals. In the present case, the atomic states are multipolar SP modes associated with the individual spheres. These are degenerate at different m (since the individual particles are spheres), and have eigenvalues $s_\ell=\ell/(2\ell+1)$.

The band structure that results from diagonalizing the matrix (9) is expressed in terms of the variable s. Thus, the bands have the form $s_\alpha(k)$, where α labels the individual bands. These may be converted into frequencies using the relation (1). This dispersion relation will take on various forms, according to how ϵ_m (and ϵ_h) depend on ω. Here we assume that the system consists of Drude metal particles in vacuum, so that $\epsilon_h=1$ and $\epsilon_m(\omega)=1-\omega_p^2/[\omega(\omega+i/\tau)]$. If $\omega_p\tau\to\infty$, then the appropriate conversion is given by

$$\omega_\alpha(k)=\omega_p\sqrt{s_\alpha(k)}. \tag{11}$$

For $\ell=1$ there are three degenerate modes at frequency $\omega_p/\sqrt{3}$, while for $\ell\to\infty$, the modes approach the limiting value of $\omega_p/\sqrt{2}$.

If the relaxation time is finite, then the relation

$$s=\frac{1}{1-\epsilon_m/\epsilon_h}=\frac{\omega(\omega+i/\tau)}{\omega_p^2} \tag{12}$$

can be inverted to express ω as a function of s. For a real s, the corresponding ω has both a real and imaginary part. Thus, we can map an eigenvalue $s_\alpha(k)$ (where α is a band index) to a *complex* eigenvalue

$$\omega_\alpha(k)=\sqrt{\omega_p^2 s_\alpha(k)-1/(4\tau^2)}-i/(2\tau). \tag{13}$$

The imaginary part describes the damping of this mode due to the finite lifetime of the surface plasmons in the individual spheres. If $\omega_p\tau\gg 1$, this damping is small, and the shift due to the damping (as embodied in the factor $1/\tau^2$ within the square root) is even smaller. Note that we have not included radiative damping in this expression. In contrast to single-particle damping, the radiative damping depends on the particle size, being greater for larger particles. For 10 nm radius gold spheres, it has been estimated that only 1.5% of the total damping rate is due to radiative damping.[11] Also, according to Refs. 3 and 4, the radiative damping should be small for particles of such a size because of strong near-field interactions.

In the Appendix, we present an alternative formulation of the equations of motion in the time domain to obtain the SP band structure, assuming a Drude dielectric function. In this formulation, which has the advantage that it can deal with localized time-dependent driving electric fields, these radiative corrections could easily be included, as has been discussed, for example, in Ref. 3.

In order to compare with experiment, we will consider two more quantities which can be obtained from the dispersion relation $\omega(k)$: First, the k-dependent group velocity $v_g(k)$ is given by the relation

$$v_g(k)\equiv\frac{d\omega}{dk}, \tag{14}$$

and can be easily computed numerically, given $\omega(k)$. Second, we can also use Eqs. (13) and (14) to estimate the energy loss from a plasmon propagating along a chain, which is important in applications. For this purpose, we define energy decay lengths $\xi_D(k)$ for the lowest longitudinal and transverse modes, as the distance over which the energy density in the wave amplitude decreases by a factor $\exp(-1)$. If the complex band frequency is denoted $\omega_1(k)+i\omega_2(k)$, then $\xi_D(k)$ is defined by

$$\frac{\xi_D(k)}{d}=\frac{v_g(k)}{2\omega_2 d}=\frac{1}{2\omega_2}\frac{d\omega(k)}{d(kd)}. \tag{15}$$

Note that in the case of the Drude approximation, the imaginary part of the complex band frequency does not depend on k, and thus ξ_D is just proportional to $v_g(k)$.

III. NUMERICAL RESULTS

We have diagonalized the matrix (9) to obtain the surface-plasmon band structure for various values of the parameter a/d. We include all bands up to $\ell=80$, which is sufficient to insure convergence of $s_\alpha(k)$ to within 1%. The results are shown in Fig. 1. For comparison, we also show the results of

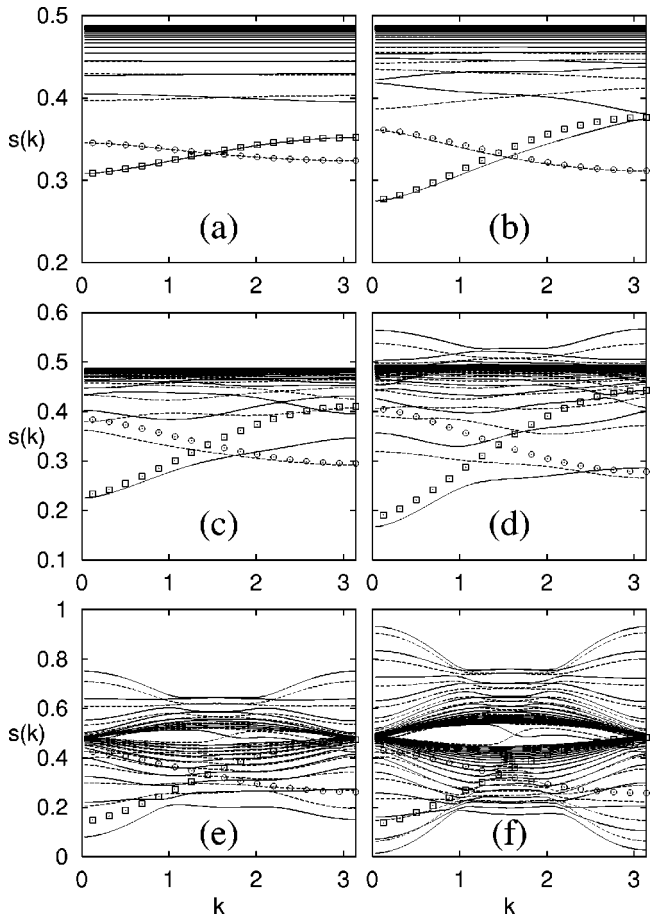

FIG. 1. Dispersion relations $s(k)$ for the surface-plasmon bands propagating along a chain of spherical nanoparticles of dielectric function ϵ_m in a host of dielectric function ϵ_h, plotted vs wave vector k. (a) $a/d=0.25$, (b) $a/d=0.33$, (c) $a/d=0.4$, (d) $a/d=0.45$, (e) $a/d=0.49$, (f) $a/d=0.5$ (spheres touching). The solid and dashed curves correspond to $m=0$ and $m=\pm 1$, respectively, for the full band structure, incorporating all bands up to $\ell=80$, as obtained diagonalizing the full Hamiltonian matrix [Eq. (9)]. The open squares ($m=0$) and circles ($m=\pm 1$) denote calculations for the $\ell=1$ modes in the dipole approximation. Note that the $m=\pm 1$ modes are degenerate.

truncating the Hamiltonian matrix at $\ell=1$. In this latter case, the Hamiltonian matrix is a diagonal 3×3 matrix with elements

$$H_{1m;1m}(k)=\frac{1}{3}+\left(\frac{a}{d}\right)^3\sum_{n=1}^{\infty}\frac{\cos(nkd)}{n^3}K_{1,1,m}, \qquad (16)$$

where $K_{1,1,0}=-4/3$ and $K_{1,1,\pm 1}=2/3$. The corresponding plasmon bands, expressed as $s_\alpha(k)$, are shown as open square ($m=0$) and circle ($m=\pm 1$) in Fig. 1. If we use the Drude expressions $\omega_\alpha^2(k)=\omega_p^2 s_\alpha(k)$, then these correspond exactly to the dipolar SP band structures obtained in Ref. 3. This behavior is as expected, since when we retain only the $\ell=1$ terms in the Hamiltonian, we are neglecting all the quasistatic contributions except the dipole fields.

As is evident, the plasmon bands take on quite a different form when the higher values of ℓ are included in the Hamiltonian matrix. For small values of a/d (i.e., $a/d\lesssim 0.3$), the lowest three bands are very similar to the bands obtained when only the $\ell=1$ matrix elements are included. This behavior is not surprising, since at these values of a/d the matrix elements connecting the $\ell=1$ states to those of higher ℓ are quite small, for any value of k. This smallness originates in the factors of $(a/d)^{\ell+\ell'+1}$ which appear in all the expressions for the matrix elements. The smallest factor connecting $\ell=1$ to higher ℓ is $(a/d)^4$ for $k\neq 0$, and $(a/d)^5$ for $k=0$. Thus, for relatively small values of a/d, these connecting matrix elements are substantially smaller than the diagonal ones.

When $a/d\gtrsim 0.35$, the interband matrix elements start to become substantial. When this happens, the shapes of the lowest bands start to depart significantly from the purely dipolar form seen for smaller a/d. As is evident, by the time $a/d\to 1/2$, the band structures of the lowest bands are so altered that they no longer bear any obvious relation to these dipolar band shapes. Precisely at $a/d=1/2$, the lowest state at $k=0$ reaches the limiting value $s=0$. This behavior is a percolation effect: when $a/d=1/2$, the two neighboring spheres just touch, and the entire line of spheres becomes one connected chain. Thus, one might expect that the lowest eigenvalues of this chain would resemble that of a very long cylinder, which indeed has as its lowest eigenvalue $s=0$.

The band structure also acquires a striking symmetry near $a/d=1/2$. First, there appears to be a nearly perfect reflection symmetry about the line $s=1/2$. In addition, there is another reflection symmetry about the line $k=\pi/(2d)$, i.e., at the middle value of k in the first Brillouin zone. As particular examples of these symmetries, there appear to be eigenvalues of $s=0$ and $s=1$ at $k=\pi/d$, just as there are at $k=0$. We do not fully understand the reasons for these symmetries. The $s\sim 0$ eigenvalue at $k=\pi/d$ apparently corresponds to a longitudinal mode (dipole moment of the spheres parallel to the z axis) in which each sphere oscillates 180° out of phase with its neighbors. The multitude of modes near $s=1/2$ presumably originate in the high-ℓ "atomic" modes, which have eigenvalues approaching $s=1/2$.

In Fig. 2, we show the eigenvalues of the two lowest bands at $k=0$ plotted as a function of a/d. Here, the lowest band corresponds to longitudinal mode ($m=0$) and the second lowest band to degenerate transverse modes ($m=\pm 1$). We performed two different calculations: In the first calculation, shown as open circles and squares, we assumed the dipole approximation and included only the $\ell=1$ part of the Hamiltonian matrix. This calculation corresponds to the tight-binding approximation used in Ref. 3. In the second, we included all bands up to $\ell=80$, which is sufficient to ensure the convergence of these two bands, as in Fig. 1, and this inclusion of the higher multipoles starts to make a substantial difference for $a/d\gtrsim 0.35$.

The inset to Fig. 2 shows the splitting Δs between the longitudinal and transverse modes at $k=0$, plotted as a function of a/d. In the dipole approximation (dashed line), this splitting increases monotonically as a/d increases.[12] However, as shown by the solid line in the inset, when the higher

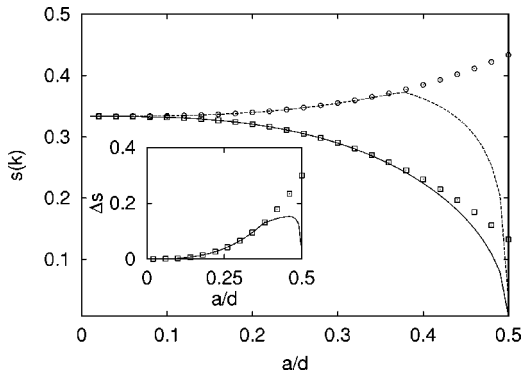

FIG. 2. Eigenvalues $s(k)$ for the lowest two bands of the band structure shown in Fig. 1 at $k=0$, evaluated as a function of a/d. Solid and dashed curves correspond to $m=0$ and $m=\pm 1$, respectively, for full multipole calculations. Open squares ($m=0$) and circles ($m=\pm 1$) are point-dipole calculations. Inset: Splitting Δs between lowest $m=\pm 1$ and $m=0$ bands at $k=0$ as calculated in the dipole approximation (open squares) and using full Hamiltonian matrix (solid line).

multipoles are included, the splitting reaches a maximum near $a/d=0.46$, then decreases again.

In order to compare with experiment, one needs to reexpress the band structure as dispersion relations for $\omega(k)$ rather than $s(k)$, using Eq. (1). With the resulting $\omega(k)$, we can also obtain $v_g(k)$ from Eq. (14) and ξ_D from Eq. (15). We show the resulting dispersion relations $\omega(k)/\omega_p$ in Fig. 3(a), and the resulting $\xi_D(k)$ and $v_g(k)$ in Fig. 3(b) for the lowest longitudinal and transverse bands as a function of kd. We denote these results as open square and circle for $a/d=0.33$, the value used in experiments, and also as solid and dashed lines for $a/d=0.45$, which is near the maximum of the splitting Δ's. In order to calculate $\omega(k)/\omega_p$, we choose $\omega_p=6.79\times 10^{15}$ rad/s and $\tau=4$ fs, as used in Ref. 7. This choice allows us to compare the present result for $a/d=0.33$ with those given in Refs. 5 and 7.

First, we compare our results for $a/d=0.33$ with experiment. For $a/d=0.33$, the result of the full calculation for $\omega(k)$ is not significantly different from the dipole approximation, since multipole effects produce only a minor alteration to the lowest bands in this case. However, the multipole effects can be seen much more clearly in the k-dependent group velocity $v_g(k)$ for these bands, and this quantity can be easily computed numerically, using the $\omega(k)$ shown in Fig. 3(a). In contrast to the result from the dipole approximation of Ref. 3, the maximum in v_g for $a/d=0.33$ does not occur at $k=\pi/(2d)$, but instead around $k=\pi/(4d)$, when the multipolar corrections are included. However, if we assume $d=75$ nm, $\omega_p=6.79\times 10^{15}$ rad/s, and $\tau=4$ fs as in Ref. 7, the *magnitude* of the maximum v_g for the longitudinal ($m=0$) mode is approximately 1.9×10^7 m/s, which is close to the result of Ref. 7, while the magnitude of v_g for the transverse ($m=\pm 1$) modes is slightly larger than the value (1.1×10^7 m/s) estimated in Ref. 7. Also, the values of ξ_D in the lowest longitudinal and transverse modes for $a/d=0.33$ are comparable to the experimental values for gold, as given in Ref. 6.

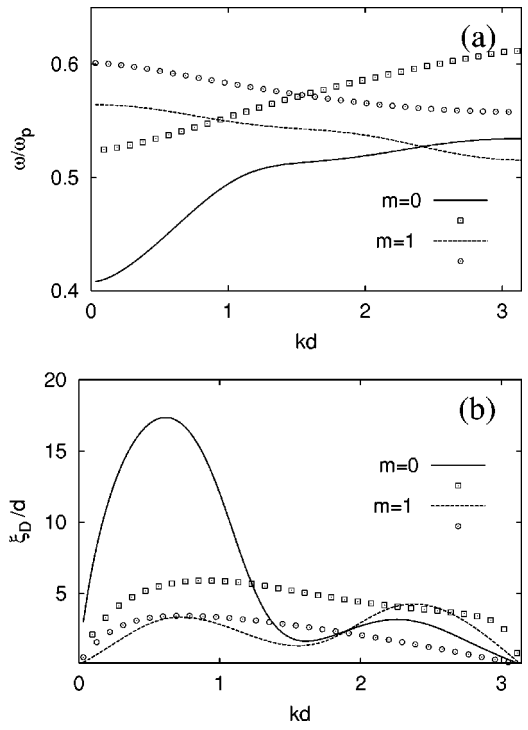

FIG. 3. (a) Dispersion relations $\omega(k)$ for the lowest two bands in a chain of metallic nanoparticles at $a/d=0.33$ or 0.45. The solid ($m=0$) and dashed ($m=\pm 1$) lines correspond to $a/d=0.45$; the open squares ($m=0$) and circles ($m=\pm 1$), to $a/d=0.33$. The curves are computed using the full Hamiltonian up to $\ell=80$, using a Drude dielectric function for the metal. (b) Energy decay lengths ξ_D, in units of the lattice constant d, and corresponding group velocities v_g in units of $\omega_p d$, plotted vs kd for the lowest two bands, assuming $a/d=0.33$ or 0.45. The labeling of the curves follows the notation of Fig. 3(a).

For $a/d=0.45$, which is near the maximum of the splitting Δs, the multipole corrections to the band structure are much greater. As a/d approaches the maximum splitting between longitudinal ($m=0$) and transverse ($m=\pm 1$) modes, the variation of v_g with k becomes nonmonotonic. In contrast to the dipole approximation, which gives a maximum group velocity at $k=\pi/(2d)$, our exact calculation actually gives a local *minimum* in v_g for this value of k (for both polarizations). As can be seen from Fig. 3(b), $v_g(k)$ has, in fact, two maxima as a function of k for this separation, for both longitudinal and transverse modes. The maximum estimated exponential decay length shown in Fig. 3(b), for the optimum k, corresponds to an $m=0$ wave, and is about three times larger than that for $a/d=0.33$. But this decay length is calculated for a wave with k vector corresponding to the maximum group velocity. The actual v_g is strongly k dependent, especially for the larger a/d. Thus, a typical wave, which would likely propagate as a packet of many different wave vectors, would likely have a quite different decay length, and also would probably not decay exponentially. It is possible that this k dependence is related to the nonexponential spatial decay of SP's found in the numerical simulations of Ref. 1.

We have not commented thus far about the role of the higher SP bands. For values of a/d greater than about 0.33,

most of these bands are nearly dispersionless, with eigenvalues $s_\alpha(k) \sim 1/2$. The SP modes corresponding to these bands will thus propagate with very small group velocity $v_{g,\alpha} = d\omega_\alpha(k)/dk$, and are likely to contribute very little to energy transport along the chain.

IV. DISCUSSION

In this work, we have calculated the surface-plasmon dispersion relations for a one-dimensional chain of spherical particles in a uniform host. In contrast to previous work, we have included all the multipolar terms in our calculation within the quasistatic approximation. We find that the dipole approximation is reasonably accurate for $a/d \leqslant 1/3$, but becomes increasingly inaccurate for larger a/d. When $a/d \rightarrow 1/2$, the lowest band shapes are entirely different from the point-dipole predictions. Thus, an accurate comparison of theory to experiment should take into account these corrections, when a/d exceeds about 1/3.

In our results near $a/d = 1/2$ we see conspicuous percolation effects. Specifically, the $k=0$ mode approaches zero frequency for a chain of Drude spheres in an insulating host. Furthermore, when $a/d \rightarrow 1/2$, the entire band structure shows remarkable reflection symmetry, both around $k = \pi/(2d)$ and around the frequency midpoint at $s = 1/2$. We do not presently understand the reasons for this symmetry.

Besides producing shape distortions in the lowest bands, the present calculations also lead to an infinite number of higher propagating SP bands. We believe, however, that these will contribute little to energy propagation, because they are characterized by much lower group velocities than the lowest two bands.

Our calculations in Fig. 3 have, of course, been carried out in the Drude approximation. As mentioned earlier, we used values of $1/\tau$ and ω_p as best fits to experiments on bulk gold, as described in Ref. 7. In actuality, the complex dielectric functions of silver, and especially gold, have substantial interband contributions, and cannot be described by a Drude dielectric function in the visible. An accurate translation of the SP band structure from the variable s to the variable $\epsilon_m(\omega)/\epsilon_h$ should use this more accurate dielectric function, e.g., by using a fit of the experimental $\epsilon_m(\omega)$ to a sum of free-electron and Lorentz oscillator parts. This more complicated procedure might somewhat change the plasmon band structures, especially for gold. Another possible complication is that, in typical experiments, the nanoparticle chains are laid down on a substrate, whose dielectric constant differs from that of vacuum. Thus, the chain is not really embedded in a homogeneous dielectric. Some workers have taken this complication into account by treating the host as homogeneous but with a dielectric function which is an average over the air and substrate dielectric functions.[5] Once again, this correction, if included, would also modify the calculated SP band structure.

The present work could be readily be generalized to higher dimensions, e.g., to an ordered layer of spheres deposited on a substrate. This extension should be straightforward, since the matrix elements required are the same as used here. The same approach could also be applied to particles of different shapes, e.g., ellipsoids or short cylinders, although the calculation of the single-particle eigenstates and the overlap integrals might be more difficult. We plan to carry out some of these extensions in the near future.

ACKNOWLEDGMENTS

This work was supported by NSF Grant No. DMR01-04987, and benefited also from the computational facilities of the Ohio Supercomputer Center.

APPENDIX: FORMULATION IN THE TIME DOMAIN

If the small spherical particles are described by a Drude dielectric function, the SP band structure can be also obtained, in perhaps a more intuitive way, by writing down a set of coupled equations of motion in *time* for the multipole moments. We first introduce the scalar quantities $q_{n\ell m}$, defined as the (ℓm)th multipole moment of the nth particle. Then, in the absence of damping, the coupled equations of motion can be written in the form

$$\ddot{q}_{n\ell m} = -\omega_{\ell m}^2 q_{n\ell m} + \omega_p^2 \sum_{\ell' m' n'}{}' \; Q_{n\ell m;n'\ell' m'} q_{n'\ell' m'}, \tag{A1}$$

where the prime over the sum indicates a sum only over the grains $n' \neq n$. For spherical grains, the single-grain resonant frequencies are given by

$$\omega_{\ell m}^2 = \frac{\ell}{2\ell+1}\omega_p^2, \tag{A2}$$

and the coupling constants $Q_{n\ell m;n'\ell' m'}$ are given by Eq. (3). Equation (A1) is readily solved for the eigenfrequencies by substituting assumed solutions of the form

$$q_{n\ell m}(t) = \mathrm{Re}[q_{\ell m} \exp(inkd - i\omega_\alpha t)] \tag{A3}$$

into Eq. (A1). Here $q_{\ell m}$ is the amplitude of the (ℓm)th multipole in a propagating mode of wave vector k. With this substitution, Eq. (A1) reduces to a set of coupled homogeneous linear algebraic equations. A solution is obtained if the determinant of the matrix of coefficients vanishes. This condition is equivalent to that of Eqs. (8), (9), and (11).

Equation (A1) has a straightforward physical interpretation. The right-hand side of Eq. (A1) describes two contributions to the force acting on the multipole moment $q_{n\ell m}$. The first term is the restoring force due to charge motion within a single particle. The second term on the right comes from the electric fields of all the multipole fields from the other particles, evaluated at the position of the nth particle. Damping is easily included in Eq. (A1) by adding to the right-hand side the term $-\dot{q}_{n\ell m}/\tau$. To obtain solutions in the presence of damping, we assume the form (A3) but with a *complex* frequency $\omega_\alpha(k) = \omega_1 + i\omega_2$. The resulting $\omega_\alpha(k)$ is given by Eq. (13).

An appealing feature of Eq. (A1) is that one can easily add a driving term. For example, if a uniform electric

field $\mathbf{E}_n(t)$ is applied to the nth grain, the interaction energy between that field and the nth grain would be $H' = -\mathbf{p}_n \cdot \mathbf{E}_n(t)$, where $\mathbf{p}_n$ is the dipole moment of the nth grain. To calculate the force on the nth grain, we write $\mathbf{p}_n = q\mathbf{x}_n$, where q is the total electronic charge in the nth grain, and $\mathbf{x}_n$ is its displacement from its equilibrium position. The interaction energy between this charge and the applied field is thus $-q\mathbf{x}_n \cdot \mathbf{E}_n(t)$. The corresponding force on the charge is just $q\mathbf{E} = M\ddot{\mathbf{x}}_n$, where M is the total mass of the electronic charge in the grain. Thus, $\ddot{\mathbf{p}}_n = q\ddot{\mathbf{x}}_n = q^2/M\mathbf{E} = (4\pi a^3 n_e e^2/3m_e)\mathbf{E} = (a^3\omega_p^2/3)\mathbf{E}$, where $m_e = 3M/(4\pi a^3 n_e)$ is the electron mass, $e = 3q/(4\pi a^3 n_e)$ is the magnitude of the electron charge, n_e is the electron density, and $\omega_p^2 = 4\pi n_e e^2/m_e$ is the squared plasma frequency.

Finally, to incorporate the damping and driving terms into the right-hand side of Eq. (A1), we express the applied electric field in terms of the spherical components $m = 0$ and $m = \pm 1$. Thus, we write $E_{n,1,0}(t) = E_{n,z}(t)$, $E_{n,1,\pm 1}(t) = E_{n,x}(t) \pm E_{n,y}(t)$. We then obtain the following equations of motion:

$$\ddot{q}_{n\ell m} = -\omega_{\ell m}^2 q_{n\ell m} - \frac{1}{\tau}\dot{q}_{n\ell m} + \frac{\omega_p^2 a^3}{3} E_{n,1,m}(t)\,\delta_{\ell,1} + \omega_p^2 \sum_{n'\ell'm'}{}' \; Q_{n\ell m;n'\ell'm'} q_{n'\ell'm'}. \tag{A4}$$

Equation (A4) is generalization of the equations written down in Ref. 3 which include all multipole moments, within the quasistatic approximation, and single-grain damping within the Drude approximation. They also include the effects of a uniform but time-dependent electric field applied to the nth nanoparticle.

Finally, we note that we have not included radiative corrections to the calculated SP bands. However, the present work could also be extended beyond the quasistatic approximation to include radiative corrections, in a simple manner, by adding an additional imaginary part to the eigenvalues. These corrections could easily be included within the dipole approximation, as has been discussed, for example, in Ref. 3.

[1] M. Quinten, A. Leitner, J.R. Krenn, and F.R. Ausenegg, Opt. Lett. **23**, 1331 (1998).

[2] J.R. Krenn, A. Dereux, J.C. Weeber, E. Bourillot, Y. Lacroute, J.P. Goudonnet, G. Schider, W. Gotschy, A. Leitner, F.R. Ausenegg, and C. Girard, Phys. Rev. Lett. **82**, 2590 (1999).

[3] M.L. Brongersma, J.W. Hartman, and H.A. Atwater, Phys. Rev. B **62**, R16356 (2000).

[4] S.A. Maier, M.L. Brongersma, P.G. Kik, S. Meltzer, A.A.G. Requicha, and H.A. Atwater, Adv. Mater. (Weinheim, Ger.) **13**, 1501 (2001).

[5] S.A. Maier, P.G. Kik, and H.A. Atwater, Appl. Phys. Lett. **81**, 1714 (2002); S.A. Maier, M.L. Brongersma, P.G. Kik, and H.A. Atwater, Phys. Rev. B **65**, 193408 (2002).

[6] S.A. Maier, P.G. Kik, H.A. Atwater, S. Meltzer, E. Harel, B.G. Koel, and A.A.G. Requicha, Nat. Mater. **2**, 229 (2003); J.R. Krenn, *ibid.* **2**, 210 (2003).

[7] S.A. Maier, P.G. Kik, and H.A. Atwater, Phys. Rev. B **67**, 205402 (2003).

[8] S.K. Gray and T. Kupka, Phys. Rev. B **68**, 045415 (2003).

[9] See, e.g., U. Kreibig and M. Vollmer, *Optical Properties of Metal Clusters* (Springer-Verlag, Berlin, 1995), p. 23.

[10] D.J. Bergman, Phys. Rev. B **19**, 2359 (1979).

[11] C. Sönnichsen, T. Franzl, T. Wilk, G. von Plessen, J. Feldmann, O. Wilson, and P. Mulvaney, Phys. Rev. Lett. **88**, 077402 (2002).

[12] J.M. Gérardy and M. Ausloos, Phys. Rev. B **25**, 4204 (1982).